

# Determination of the Solid-Liquid Interface Energy in the Al-Cu-Ag System

A. BULLA, C. CARRENO-BODENSIEK, B. PUSTAL, R. BERGER,  
A. BÜHRIG-POLACZEK, and A. LUDWIG

The solid-liquid interface energy,  $\sigma_{SL}$ , is of major importance during phase transformation. It has a strong influence on solidification morphologies and the final grain structure. The “grain boundary groove in an applied temperature gradient” method developed by Gündüz *et al.*<sup>[6]</sup> was found to be suitable for measuring the solid-liquid interface energy in ternary alloy systems (*e.g.*, Al-Cu-Ag). In order to measure the solid-liquid interface energy, a radial heat flow apparatus was constructed and assembled. This apparatus ensures a stable temperature gradient for hours and leads to grain boundary grooves in chemical equilibrium. After rapid quenching, the samples were metallographically prepared and the local curvature of the grooves was analyzed. To determine the interface energy, the Gibbs–Thomson equation was used, which requires the local curvature of the grain boundary grooves and the adherent local undercooling obtained from heat flux simulations on the scale of the grooves.

DOI: 10.1007/s11661-007-9275-6

© The Minerals, Metals & Materials Society and ASM International 2007

## I. INTRODUCTION

THE objective of this article is to point out a methodology for measuring the solid-liquid interface energy,  $\sigma_{SL}$ , for ternary alloy systems, *e.g.*, Al-Cu-Ag with an invariant eutectic composition.

The solid-liquid interface energy plays a central role during solidification processes, *i.e.*, phase nucleation, additional growth, and the resulting morphology (cellular, dendritic, or globular). In addition to chemical diffusion, it is this quantity that governs the microstructure length scale. Therefore, the solid-liquid interface energy is an important parameter in many solidification models. Unfortunately, there is no direct method known for measuring the solid-liquid interface energy in metallic systems. For binary alloys, the literature provides only limited experimental data, and no values have yet been determined for the solid-liquid interface energy of multicomponent systems. In the present work, the solid-liquid interface energy was measured for the first time, for an alloy with an invariant eutectic composition in the ternary system Al-Cu-Ag.

One of the most common techniques for measuring the solid-liquid interface energy is the “grain boundary groove in an applied temperature gradient” method. Gündüz<sup>[6]</sup> developed a radial heat flow apparatus for establishing a temperature gradient using a single heating wire along the axis of a cylindrical sample and

a water-cooling jacket on the outside of the sample. The authors used the radial heat flow apparatus to measure the solid-liquid interface energies for different binary alloy systems,<sup>[1–8]</sup> by observing the equilibrated grain boundary groove shapes.

The solid-liquid interfaces of two grains were equilibrated in a stable temperature gradient for a time sufficient to produce a macroscopically planar solid-liquid interface, except where grain boundary cusps were formed. After quenching, the interface energy was obtained indirectly, using the Gibbs–Thomson equation. The Gibbs–Thomson equation requires measuring the local curvature of the grain boundary grooves, determining the local undercooling by heat flux simulations, and understanding the entropy of fusion, to obtain the solid-liquid interface energy. In this work, the radial heat flow apparatus was first applied to reproduce the previous results of Gündüz for an eutectic Al-Cu alloy. In additional experiments, the solid-liquid interface energy in the ternary system Al-Cu-Ag was determined.

## II. EXPERIMENTAL PROCEDURE

### A. The Radial Heat Flow Apparatus

The radial heat flow apparatus needed to be constructed such that a constant radial temperature gradient could be established by using a single heating wire along the axis of the cylindrical sample and a water-cooled jacket at the outside of the sample, as shown in Figure 1. To prevent a horizontal convectional flow, only a thin liquid layer (1- to 2-mm thick) was melted along the ceramic tube surrounding the central heating element. The semisolid samples were held in a stable radial temperature gradient for about 4 days—depending on

---

A. BULLA, B. PUSTAL, and R. BERGER, Scientific Assistants, C. CARRENO-BODENSIEK, Associate Professor, and A. BÜHRIG-POLACZEK, Director, are with the Foundry Institute, RWTH Aachen University, Aachen D-52072, Germany. Contact e-mail: a.bulla@gi.rwth-aachen.de A. LUDWIG, Professor and Head of Chair for Simulation and Modelling of Metallurgical Processes, is with the Department of Metallurgy, University of Leoben, Leoben A-8700, Austria.

Manuscript submitted January 21, 2007.

Article published online July 31, 2007.

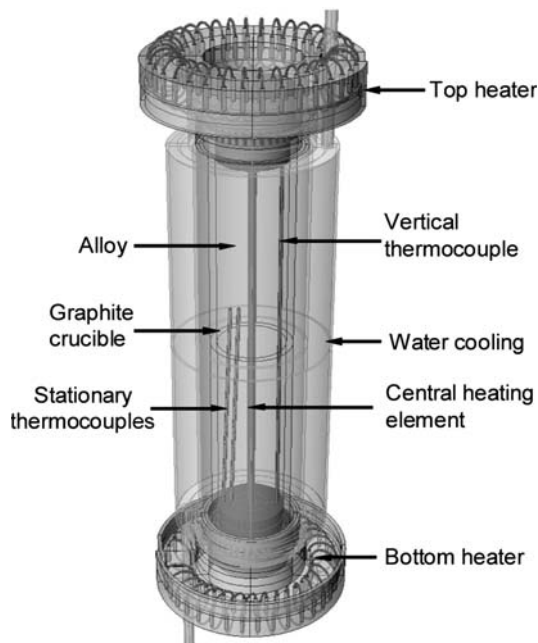


Fig. 1—Schematic illustration of the radial heat flow apparatus consisting of the graphite crucible, the central heating element, and the cooling jacket with the top and bottom heaters.

the alloy—until all diffusion fluxes were terminated, *i.e.*, no macroscopic concentration profiles existed in the grains and liquid at the interface. A chemical equilibrium state was reached and the interface energy, which is to be determined, is the only off-equilibrium effect. After the equilibration process of the sample, the shape of the cusps was conserved by rapid quenching.

### B. Equilibration of a Sample

The experiments were carried out in three steps. In the first step, the thermocouples were calibrated by slow heating and cooling, detecting the known transformation temperature at the invariant eutectic composition. In order to equilibrate the sample, the temperature was set such that a thin liquid layer (1 to 2 mm) melted along the central heating element. With the horizontal temperature gradient kept constant, the sample was placed in the radial heat flow apparatus until the grain boundary grooves were in chemical equilibrium. During the annealing, the mean temperature deviation was about  $\pm 0.02$  °C for 1 hour and  $\pm 0.05$  °C for 4 days. After equilibration, the shape of the cusps was preserved by rapid quenching. The quenching was done by turning off the input power of the central heating element and of the top and bottom heaters, and simultaneously cooling the outside of the sample. The samples were left in the radial heat flow apparatus until they were cooled down to room temperature. From the chart trace (Figure 2), it was estimated that, at the beginning of the quenching process, the cooling rate at the control thermocouple was about 30 (°C/min), which was sufficient to get a well-defined solid-liquid interface.

## III. EVALUATION OF THE LOCAL CURVATURE OF THE GRAIN BOUNDARY GROOVE

### A. Preparation of Specimens

The cylindrical sample was cut in a transverse direction, in 20-mm slices. The microexamination of the sample was done using a light optical microscope. After metallographic preparation (embedding, grinding, and polishing), the specimens were etched with molybdic acid. To determine the orientation of the grain boundary grooves relative to the polished surface, two cross-sectional cuts with a defined distance were required (Figure 3).

Two perpendicular reference lines (approximately 200- $\mu$ m thick and 350- $\mu$ m deep) were set near the grain boundary groove on the polished surface of the specimen, using a milling cutter to obtain a global reference frame. The thickness of the specimen after grinding,  $d$ , was measured using a digital micrometer. Because of considerable deviations in the measurements, a new method had to be found to determine the amount of abrasion in the specimen. Four opposite center holes (approximately 1.0- to 1.5-mm thick and 350- $\mu$ m deep) were drilled into the polished surface of the specimen, with a drill bit angle of 90 deg (Figure 4(a)). From the variation in the diameter, the amount of abrasion in the second plane compared to the first plane could be deduced (Figure 4(b)).

After the metallographic preparation, the specimens were photographed using a charge-coupled device (CCD) camera connected to the microscope by a magnification factor of 50, in a series of up to 80 pictures, to obtain an overview by joining the individual pictures using graphic manipulation software (Figure 3).

### B. Measurement of the Grain Boundary Groove Coordinates

The grain boundary grooves were photographed at a magnification of 500, to allow an accurate measurement of the local curvature of the grooves (Figure 5). The  $x$  and  $y$  coordinates of the grain boundary grooves were determined using computer-aided design (CAD) software.

### C. Geometrical Correction of the Groove Coordinates

In general, it is assumed that, in the order of magnitude of the grain, no curvature exists along the direction of the cusp line ( $z$ -direction) of the grain boundary groove. Due to translation invariance in this direction, the three-dimensional geometry of the grain boundary groove can be reduced to a two-dimensional one by a projection on a plane orthogonal to the cusp line. In this two-dimensional geometry, the grain boundary groove is represented by a curve. The curvature at any point of the curve is identical to the curvature at the points of the three-dimensional grooves. Since the polished surfaces of the specimens are not perpendicular to the surfaces of the grain boundary groove (Figure 6), a transformation of the  $x$  and  $y$  coordinates of the grain boundary groove is necessary.

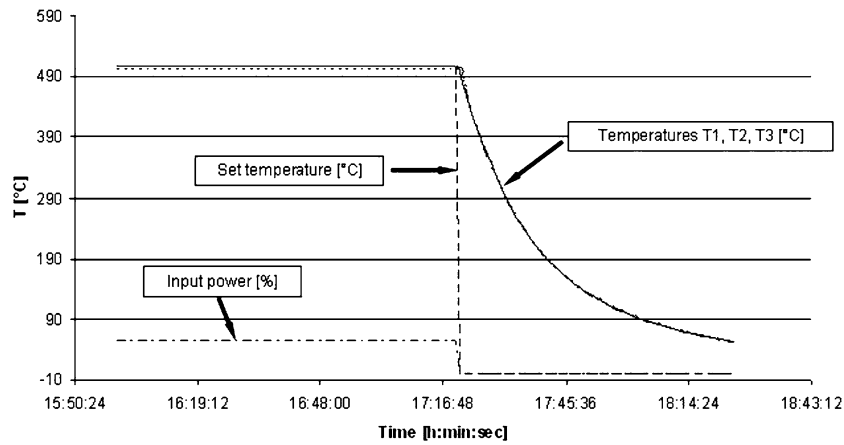


Fig. 2—Rapid quenching of the sample occurs by turning off the input power.

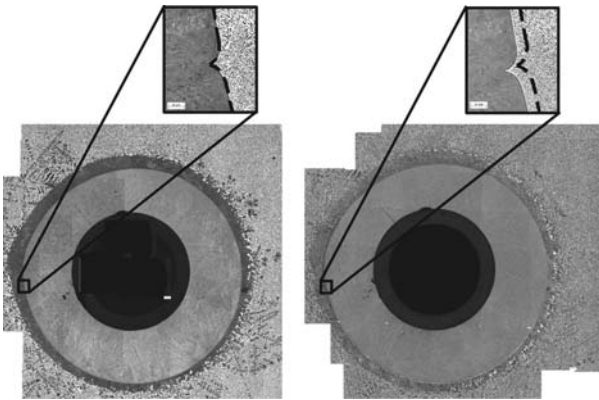


Fig. 3—Overview of two cross sections of a specimen with a defined distance,  $d$ , of an eutectic Al-Cu-Ag alloy consisting of 50 single pictures magnified 50 times (left: first plane, and right: second plane).

The coordinates of the cusps,  $x'$ ,  $y'$ , from the metallographic section must be projected into an  $x$ -,  $y$ -,  $z$ -coordinate system aligned with the grain. This new coordinate system is oriented such that the  $z$ -axis is parallel to the base of the grain boundary groove and the  $y$ -axis is perpendicular to the macroscopic solid-liquid interface plane. The measured  $x'$ ,  $y'$  coordinates

are then projected onto the  $z = 0$  plane in the coordinate system of the grain. This transformation is a prerequisite for a correct determination of the interface curvature and for the simulation of the adherent undercooling.

For the transformation of the measured geometry, the exact position according to the global reference frame and the orientation of the grain boundary grooves according to the two cross sections, with a defined distance of about 40 to 50  $\mu\text{m}$  in the specimen, is required (Figure 6).

Overviews of the two cross sections were aligned to one another and superimposed, to measure the displacement of the solid-liquid interface along the  $y'$ -axis and to determine the displacement of the grain boundary groove position along the  $x'$ -axis. Figure 6 schematically shows the position of the new coordinate system relative to the two cross sections and the superimposed boundary groove shapes of the two cross sections.

In accordance with Maraşlı,<sup>[1-4]</sup> an arbitrary spatial position of the groove shape relative to the cross sections was assumed. The position of the new coordinate system  $x$ ,  $y$ ,  $z$ , which is aligned to the groove, was determined by the lengths  $a$ ,  $b$ , and  $d$ . A projection onto a plane perpendicular to the base line of the grain boundary groove was then carried out (Figure 7).

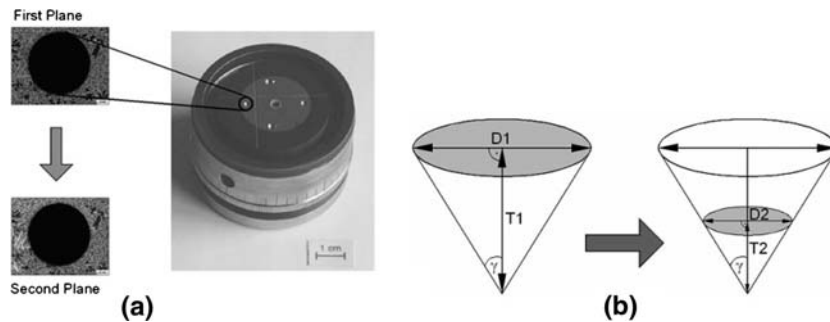
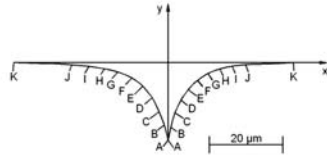
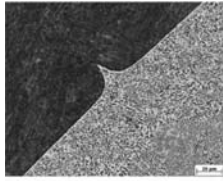


Fig. 4—(a) Changes in diameter of the center holes after grinding. (b) The half angle at the tip of the drill bit,  $\gamma$ , was used to determine the amount of abrasion,  $d$ , where  $D$  is the diameter of the drill holes at the surface.



Point	Left		Right	
	X	Y	X	Y
A	0	-20.70	0	-20.70
B	-0.63	-17.89	0.63	-18.10
C	-1.18	-15.26	1.27	-15.72
D	-2.08	-12.19	2.08	-13.23
E	-3.49	-9.53	3.17	-10.62
F	-5.53	-7.04	5.15	-7.38
G	-8.32	-4.62	7.66	-4.90
H	-11.35	-2.83	10.44	-3.38
I	-15.66	-1.49	13.67	-2.35
J	-19.81	-0.92	17.42	-1.45
K	-30.16	0	36.77	0

$G_S = 4.512 [^{\circ}C/cm]$ ,  $R_{M(a)} = K_L/K_S = 0.362$

Fig. 5—Measurement of the  $x$  and  $y$  grain boundary groove coordinates, using CAD software.

The transformation can be expressed as

$$x = x' \frac{\sqrt{a^2 + d^2}}{\sqrt{a^2 + b^2 + d^2}} + y' \frac{-ab}{\sqrt{a^2 + d^2} \sqrt{a^2 + b^2 + d^2}} \quad [1]$$

and

$$y = y' \frac{d}{\sqrt{a^2 + d^2}} \quad [2]$$

where  $a$  is the displacement of the solid-liquid interface along the  $y'$ -axis,  $b$  is the displacement of the grain boundary groove position along the  $x'$ -axis, and the distance  $d$  describes the amount of abrasion along the  $z'$  axis, which was calculated from the average values of the diameter change of the four center holes (Figure 4).

$$d = \frac{D_1 - D_2}{2 \tan \gamma} \quad [3]$$

where  $\gamma$  is half of the angle of the tip of the drill bit and  $D$  is the diameter of the drill holes, with respect to the first and second plane.

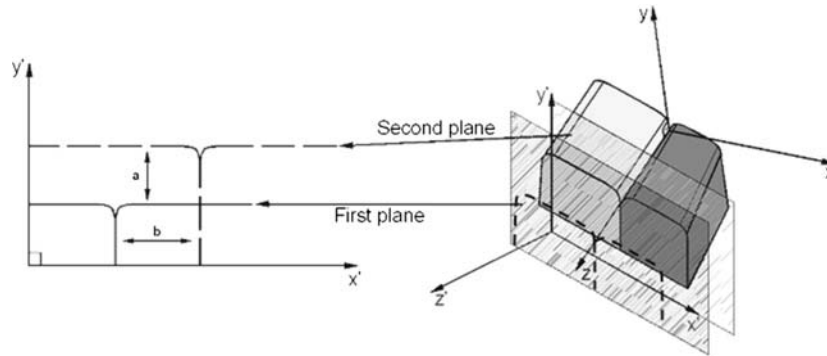


Fig. 6—Schematic drawing to show the relation between the coordinate systems of the grain and of the ground cross section.<sup>[1-4]</sup>

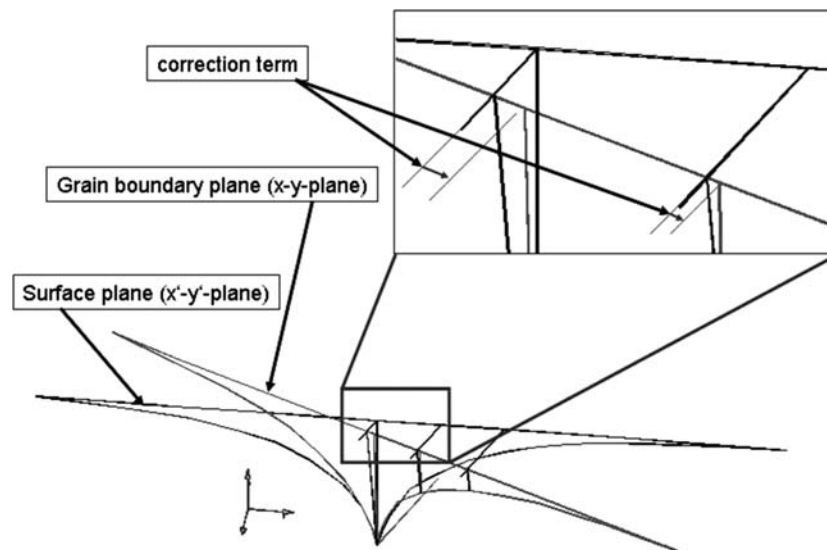


Fig. 7—Vectorial projection of the grain boundary groove from the polished surface plane onto the grain boundary plane.

#### D. Determination of the Local Undercooling

Assuming that the liquid and the solid have the same thermal conductivities, the local undercooling is merely a function of the measured gradient and the  $y$ -coordinate. If the solid and liquid phases have different thermal conductivities, the isotherms at the grain boundary groove cusps are deformed and the local undercooling has to be determined numerically. Figure 8 shows an example of a numerical simulation of the microscopic temperature field, to determine the local deformation of the isotherms at the grain boundary groove, e.g., for the theta phase in an eutectic Al-Cu-Ag alloy.

The shape of the solid-liquid interface was extrapolated using the transformed experimental groove shapes. Dirichlet boundary conditions, i.e., fixed temperatures, have been set at the bottom (775.0 K) and at the top (775.2 K) of the domain, deduced from the macroscopic temperature gradient measured during the equilibration experiment. On either side of the domain, a homogeneous Neumann condition was set, i.e., the lateral heat flux is zero. The following material data were used: Thermal conductivities:  $\lambda_{\theta\text{-solid}} = 110.64$  (W/K/m),  $\lambda_{\text{liquid}} = 55.357$  (W/K/m), specific heat capacity:  $C_{p/\text{liquid}} = 718.3$  (J/kg/K).<sup>[10]</sup> The thermal conductivities of the solid phases were determined experimentally, in cooperation with the “Forschungszentrum Karlsruhe” (Germany) for the present study, in 2006. The thermal conductivity of the liquid phase was determined experimentally with a unidirectional growth apparatus, in cooperation with “Access e.V” Aachen (Germany) in 2006.

The temperature field simulations were carried out using the commercial program package FLUENT<sup>®</sup> Rev. 6.1.18.\* To automate the calculation of the local

quantify the undercooling along a grain boundary groove, in order to calculate the Gibbs–Thomson coefficient.

#### E. Determination of the Solid-Liquid Interface Energy

Based on the two-dimensional geometry of the grain boundary groove obtained by the coordinate transformation (Section II–C), the Gibbs–Thomson equation, at any point of the curve of the grain boundary groove, can be expressed as

$$\Delta T_r = \frac{\Gamma}{r} \quad [4]$$

where  $r$  is the radius of the curvature at this point.

Since measuring errors can lead to huge inaccuracies in the determination of the curvature, the Gibbs–Thomson equation was not evaluated directly but in an integral form.

$$\int_{y_1}^{y_n} \Delta T_r dy = \Gamma \int_{y_1}^{y_n} \frac{1}{r} dy \quad [5]$$

The left-hand side of the equation was evaluated numerically, determining the appropriate undercooling,  $\Delta T_r$ , at a point,  $y_n$ , of the simulated temperature field, as described earlier (Figure 8).

$$\int_{y_1}^{y_n} \Delta T_r dy \approx \sum_{i=1}^{n-1} (y_i - y_{i+1}) \cdot \left( \frac{\Delta T_i + \Delta T_{i+1}}{2} \right) \quad [6]$$

The right side of Eq. [5] may be evaluated for any shape by setting the length element  $ds = r d\theta$ , where  $s$  is the distance along the interface and  $\theta$  is the angle of a tangent to the interface with the  $y$ -axis (Figure 9). Hence,  $dy = \cos(\theta) ds = \cos(\theta) r d\theta$  can be substituted in the right side of Eq. [5], which gives for an arbitrary surface

\*FLUENT<sup>®</sup> is a registered trademark of ANSYS, Inc., Lebanon, NH.

undercooling, a suitable program code was developed to

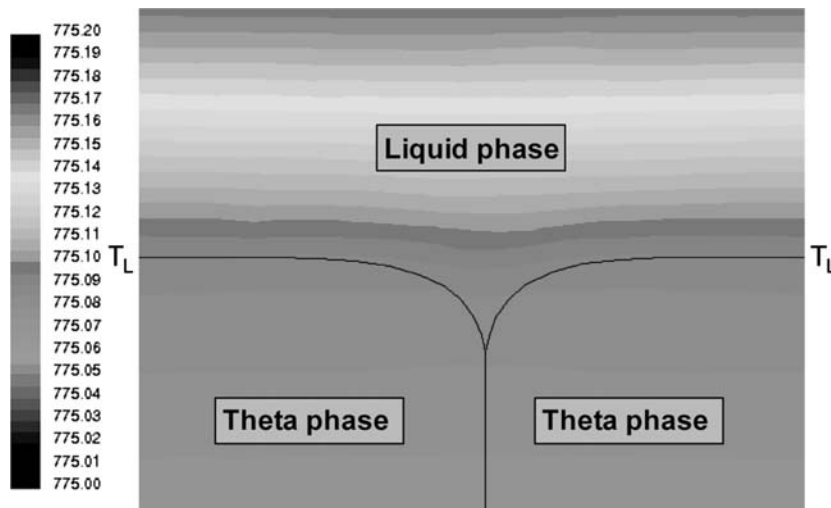


Fig. 8—Section of the temperature distribution that was numerically determined at a grain boundary groove in an Al-Cu-Ag alloy.

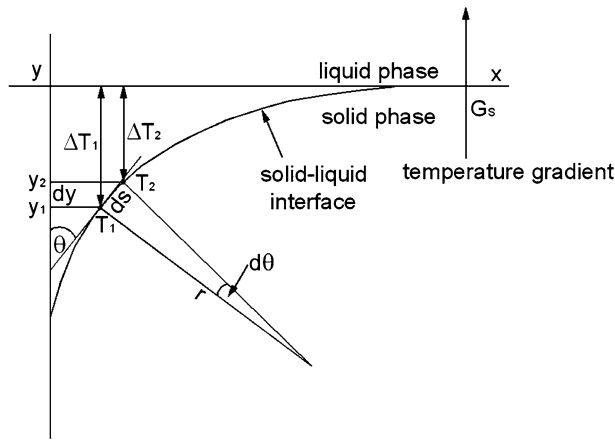


Fig. 9—Temperature difference at two different points of the grain boundary groove and description of  $ds$ ,  $d\theta$ , and  $r$ .

$$\Gamma \cdot \int_{y_1}^{y_n} \frac{1}{r} dy = \Gamma \cdot \int_{\theta_1}^{\theta_n} \frac{1}{r} \cdot r \cdot \cos(\theta) d\theta$$

$$= \Gamma \cdot (1 - \sin \theta) \Big|_{\theta_1}^{\theta_n} = \Gamma \cdot (\sin \theta_1 - \sin \theta_n)$$

[7]

This allows the Gibbs–Thomson coefficient to be calculated by numerically evaluating the right side of Eq. [5] using the undercooling temperatures from the temperature field simulations and measuring the angle  $\theta$  constructing a tangent to the surface at  $y_n$ .

The solid-liquid interface energy is obtained from the definition of the Gibbs–Thomson coefficient:

$$\Gamma = \frac{\sigma_{SL}}{\Delta S^*}$$

[8]

The term  $\Delta S^*$  is the specific entropy change per unit volume at the transformation temperature, which must be known or obtained from other sources. In this study, the entropy has been determined by Thermo-Calc (Thermo-Calc Software, Stockholm, Sweden) using the database described by Witusiewicz *et al.*<sup>[9]</sup>

#### IV. RESULTS AND DISCUSSION

Before the results for the ternary alloy systems had been obtained, the described procedure was tested to reproduce the results obtained previously by Gündüz<sup>[7]</sup> and Maraşlı<sup>[11]</sup> for a binary Al-Cu alloy with an eutectic composition. The solid-liquid interface energy could be evaluated in this study for  $\sigma_{SL \text{ Al}(x)} = 169 \text{ (mJ/m}^2\text{)}$  and the  $\sigma_{SL \text{ CuAl}_2} = 86 \text{ (mJ/m}^2\text{)}$ , and the values were in a good accordance with the results of Gündüz and Maraşlı. Afterward, experiments were carried out to determine the solid-liquid interface energy in the ternary Al-Cu-Ag system. The alloy used had an eutectic composition of 16.86 wt pct Cu and 39.97 wt pct Ag

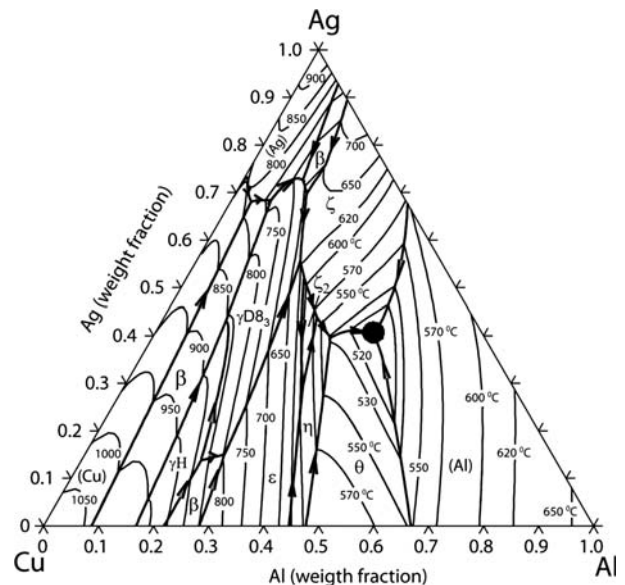


Fig. 10—Projection of the liquid surfaces with isotherms plotted in the different phase regions of the Al-Cu-Ag system. The alloy used to carry out the experiments had an eutectic composition of 43.17 wt pct Al, 16.86 wt pct Cu, and 39.97 wt pct Ag, at a temperature  $T_E = 501.94 \text{ }^\circ\text{C}$ .

at a temperature of  $501.94 \text{ }^\circ\text{C}$ , as shown in Figure 10, according to Witusiewicz *et al.*<sup>[9]</sup>

The samples were left in the radial heat flow apparatus for 4 days, with the temperature gradient kept constant until the grain boundary grooves were in local equilibrium. After quenching, the samples were cut in a transverse direction in 20-mm slices. The specimens were metallographically prepared and photographed. Along the cylindrical sample, equilibrated grain boundary grooves of the  $\text{Al}(x)$  phase, the  $\text{CuAl}_2$  phase, and the  $\text{Ag}_2\text{Al}$  phase, in equilibrium with the liquid, were observed (Figure 11). The Gibbs–Thomson coefficient was calculated, using five grooves for each phase.

##### A. Liquid in Equilibrium with the $\text{Al}(x)$ phase

In Table I, the displacement of the solid-liquid interface along the  $y'$ -axis,  $a$ , the displacement of the grain boundary groove position along the  $x'$ -axis,  $b$ , and the amount of abrasion,  $d$ , of the different phases are displayed. The temperature gradients,  $G_s$ , to the corresponding grooves are also presented.

For the numerical determination of the local undercooling, the thermal conductivities of the solid phases,  $\lambda_S$ , and the liquid phase,  $\lambda_L$ , have to be determined. The thermal conductivities of the solid phases,  $\lambda_S$ , were determined experimentally for each phase by means of the Laser-Flash method<sup>[11–13]</sup> and differential scanning calorimetry (DSC):

$$\lambda = \alpha c_p \rho$$

[9]

where  $\alpha$  is the thermal diffusivity,  $c_p$  the specific heat capacity, and  $\rho$  the density. The thermal conductivity of the liquid phase was determined experimentally by means of a unidirectional growth apparatus, *i.e.*, a Bridgman furnace.

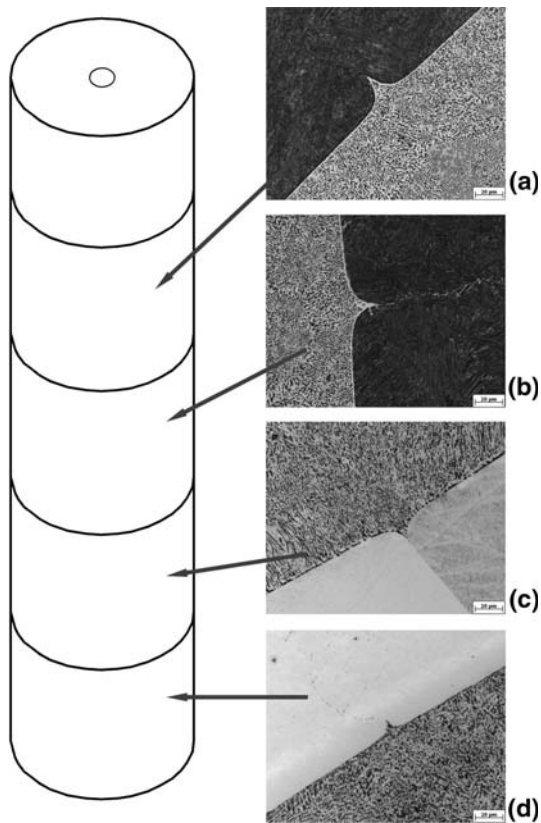


Fig. 11—Distribution of the different phases along the cylindrical sample for an eutectic Al-Cu-Ag alloy: (a) and (b): Al<sub>(α)</sub> phase, (c) CuAl<sub>2</sub> phase, and (d) Ag<sub>2</sub>Al phase, in equilibrium with the melt.

**Table I. Correction of the Grain Boundary Grooves in the *x*-Direction and *y*-Direction; the Temperature Gradient, *G<sub>s</sub>*, of the Al<sub>(α)</sub>, CuAl<sub>2</sub>, and Ag<sub>2</sub>Al Phases is in Equilibrium with the Quenched Liquid**

Phase	Groove	Displacement			<i>G<sub>s</sub></i> (K/cm)
		<i>a</i> (μm)	<i>b</i> (μm)	<i>d</i> (μm)	
Solid Al <sub>(α)</sub> -liquid Al-Cu-Ag	(a)	-10.7	-23.2	27.2	3.717
	(b)	-8.9	-18.2	27.2	3.641
	(c)	-6.9	-15.0	27.2	3.675
	(d)	-6.1	-16.9	27.2	3.706
	(e)	-0.4	-14.0	27.2	3.736
Solid CuAl <sub>2</sub> -liquid Al-Cu-Ag	(a)	4.6	-11.8	13.0	4.385
	(b)	5.0	-13.6	13.0	4.372
	(c)	-0.9	-16.5	13.0	4.372
	(d)	-1.0	-12.6	13.0	4.349
	(e)	2.7	-12.0	13.0	4.388
Solid Ag <sub>2</sub> Al-liquid Al-Cu-Ag	(a)	8.9	25.9	40.1	2.281
	(b)	7.2	54.3	40.1	2.282
	(c)	0	0	40.1	2.268
	(d)	5.9	28.7	40.1	2.317
	(e)	12.1	7.2	40.1	2.243

In Table II, the thermal conductivities of the solid phases and the liquid phase are presented.

In Table III, the results of the Gibbs–Thomson coefficient,  $\Gamma$ , and the solid-liquid interface energy,  $\sigma_{SL}$ , for the Al<sub>(α)</sub>, CuAl<sub>2</sub>, and Ag<sub>2</sub>Al phases are listed.

**Table II. Thermal Conductivity,  $\lambda_S$ , Specific Heat Capacity,  $c_p$ , and Density,  $\rho$ , of the Solid Al(Alpha), CuAl<sub>2</sub>, and Ag<sub>2</sub>Al Phases, and  $\lambda_L$ , of the Liquid Phase in the Ternary Al-Cu-Ag System**

Phase	$c_p$ (J/kg K)	$\rho$ (kg/m <sup>3</sup> )	$\lambda_S$ (W/m K)	$\lambda_L$ (W/m K)
Solid Al <sub>(α)</sub> -liquid AlCuAg	1250	4210	152.99	55.357
Solid CuAl <sub>2</sub> -liquid AlCuAg	665	4390	110.64	
Solid Ag <sub>2</sub> Al-liquid AlCuAg	414	7900	38.91	

**Table III. Results of the Gibbs–Thomson Coefficient,  $\Gamma$ , and the Solid-Liquid Interface Energy,  $\sigma_{SL}$ , of the Al<sub>(α)</sub>, CuAl<sub>2</sub>, and Ag<sub>2</sub>Al Phases in Equilibrium with the Liquid**

Phase	Groove	$\Gamma_{xy} \times 10^{-8}$ (K*m)	$\sigma_{SL}$ (mJ/m <sup>2</sup> )
Solid Al <sub>(α)</sub> -liquid Al-Cu-Ag	(a) left	7.4	80
	(a) right	5.2	56
	(b) left	4.8	52
	(b) right	4.4	47
	(c) left	5.7	62
	(c) right	5.3	57
	(d) left	7.5	81
	(d) right	8.1	87
	(e) left	7.8	84
	(e) right	6.3	68
Solid CuAl <sub>2</sub> -liquid Al-Cu-Ag	(a) left	4.2	79
	(a) right	5.9	112
	(b) left	4.5	85
	(b) right	6.9	130
	(c) left	4.6	87
	(c) right	4.9	93
	(d) left	5.8	109
	(d) right	4.6	86
	(e) left	4.1	78
	(e) right	5.6	105
Solid Ag <sub>2</sub> Al-liquid Al-Cu-Ag	(a) left	2.4	28.0
	(a) right	2.2	25.4
	(b) left	3.7	43.5
	(b) right	1.8	21.5
	(c) left	2.2	25.5
	(c) right	2.3	26.9
	(d) left	2.1	24.0
	(d) right	2.2	25.4
	(e) left	3.1	36.6
	(e) right	2.3	26.8

The average value of the Gibbs–Thomson coefficient for the solid Al<sub>(α)</sub>-liquid Al-Cu-Ag system was found to be  $\Gamma = (6.3 \pm 1.4) \times 10^{-8}$  (K\*m). The weighted entropy change per gram,  $\Delta S^*$ , for the Al<sub>(α)</sub> phase was determined using the Thermo-Calc software. The molar volume of the phase  $V_S$  was obtained from the composition and from the density of the phase (Table IV). With a specific entropy change per unit volume of  $\Delta S^* = 10.75612 \times 10^5$  (J/m<sup>3</sup>K), the solid-liquid interface energy,  $\sigma_{SL}$ , was found to be  $(67 \pm 15)$  (mJ/m<sup>2</sup>).

**Table IV. Molar Volume,  $V_S$ , and Entropy Change of the Solid  $Al_{(x)}$ ,  $CuAl_2$ , and  $Ag_2Al$  Phases in the Ternary Al-Cu-Ag System;  $\Delta S^*$  was Calculated with Thermo-Calc, and the Molar Volume Was Calculated from the Density, the Composition, and the Atom Mass of the Phases**

Solid Phase	Composition (Wt Pct)	$V_S \times 10^{-5}$ (m <sup>3</sup> /mol)	$\Delta S^*$ (J/mol K)	$\Delta S^* \times 10^5$ (J/m <sup>3</sup> K)
$Al_{(x)}$	50.41 (Al) 7.5 (Cu)	0.99943	10.75	10.75612
$CuAl_2$	42.09 (Ag) 47.00 (Al) 52.88 (Cu)	0.88449	16.70	18.88085
$Ag_2Al$	0.12 (Ag) 13.82 (Al) 2.47 (Cu) 83.71 (Ag)	0.9538	11.16	11.70052

Atom mass (kg/mol): 0.02698 (Al), 0.06354 (Cu), and 0.10787 (Ag).

The relative error for the solid-liquid interface energy was about 22 pct.

### B. Liquid in Equilibrium with the $CuAl_2$ Phase and the $Ag_2Al$ Phase

Analogous to the determination of the Gibbs–Thomson coefficient and the solid-liquid interface energy of the  $Al_{(x)}$  phase, the Gibbs–Thomson coefficient and the solid-liquid interface energy of the  $CuAl_2$  phase and the  $Ag_2Al$  phase were determined (Table III). For the solid  $CuAl_2$ -liquid Al-Cu-Ag system, an average value of the Gibbs–Thomson coefficient of  $\Gamma = (5.1 \pm 0.9) \times 10^{-8}$  (K\*m) was determined. With a specific entropy change per unit volume of  $\Delta S^* = 18.88085 \times 10^5$  (J/m<sup>3</sup>K) (Table IV), the solid-liquid interface energy,  $\sigma_{SL}$ , was found to be  $(96 \pm 17)$  (mJ/m<sup>2</sup>). The relative error for the solid-liquid interface energy was about 18 pct. For the solid  $Ag_2Al$ -liquid Al-Cu-Ag system, the average value of the Gibbs–Thomson coefficient was found to be  $\Gamma = (2.4 \pm 0.6) \times 10^{-8}$  (K\*m). The solid-liquid interface energy,  $\sigma_{SL}$ , was found to be  $(28 \pm 7)$  (mJ/m<sup>2</sup>). A specific entropy change per unit volume of  $\Delta S^* = 11.70052 \times 10^5$  (J/m<sup>3</sup>\*K) was calculated (Table IV). The relative error for the solid-liquid interface energy was about 25 pct.

## V. CONCLUSIONS

The radial heat flow apparatus in combination with the grain boundary groove in an applied temperature gradient method can be applied to measure the Gibbs–Thomson coefficient,  $\Gamma$ , and the solid-liquid interface energy,  $\sigma_{SL}$ , for grain boundary grooves in pure materials and alloys for which the groove shape can be investigated after quenching. In this method, the local curvature of the grain boundary grooves and the local undercooling by heat flux simulations must be determined using the Gibbs–Thomson equation. For the simulation of the local undercooling, the temperature gradients in the liquid and the solid phases must be known, in addition to the groove shape.

During the experiments, segregation leads to a small variation in the composition of the liquid phase, depending on the height. Hence, different phases are

observed in equilibrium with the liquid phase at different heights. In the presented work, values of the solid-liquid interface energy for a binary Al-Cu alloy with an eutectic composition were first reproduced and were in a good accordance with the previous results of Gündüz<sup>[7]</sup> and Maraşlı.<sup>[1]</sup>

In the present article, first measurements of the solid-liquid interface energy for the ternary system Al-Cu-Ag with an invariant eutectic composition were carried out. The Gibbs–Thomson coefficient,  $\Gamma$ , and the solid-liquid interface energy,  $\sigma_{SL}$ , were determined for the three phases: the  $Al_{(x)}$  phase, the  $CuAl_2$  phase, and the  $Ag_2Al$  phase. A comparison of the results of the solid-liquid interface energy for the  $Al_{(x)}$  phase shows that, in the ternary system, the value is about 2.5 times smaller than in the binary system, whereas the value for the  $CuAl_2$  phase is in the same range.

## ACKNOWLEDGMENTS

The authors express their gratitude to the German Research Foundation (Deutsche Forschungsgemeinschaft, DFG, Schwerpunktprogramm SPP 1120) for the financial support required to accomplish the studies within the DFG research focus, “Phase Transformations in Multicomponent Alloys.”

## REFERENCES

1. N. Maraşlı: Doctoral Thesis, University of Oxford, Oxford, United Kingdom, 1994.
2. N. Maraşlı and J.D. Hunt: *Acta Mater.*, 1996, vol. 44, p. 1085.
3. M. Erol, N. Maraşlı, K. Keşlioğlu, and M. Gündüz: *Scripta Mater*, 2004, vol. 51, pp. 131–36.
4. K. Keşlioğlu and N. Maraşlı: *Mater. Sci. Eng., A*, 2004, vol. 369, pp. 294–301.
5. N. Maraşlı, K. Keşlioğlu, and B. Arslan: *J. Cryst. Growth*, 2003, vol. 247, pp. 613–22.
6. M. Gündüz: Doctoral Thesis, University of Oxford, Oxford, United Kingdom, 1994.
7. M. Gündüz and J.D. Hunt: *Acta Metall.*, 1985, vol. 33 (9), pp. 1651–72.
8. M. Gündüz and J.D. Hunt: *Acta Metall.*, 1989, vol. 37 (7), p. 1839.

9. V.T. Witusiewicz, U. Hecht, S.G. Fries, and S. Rex: *J. Alloys Compd.*, 2005, vol. 387, pp. 217–27.
10. Y.S. Touloukian and C.Y. Ho: *Thermophysical Properties of Matter, Specific Heat Metallic Elements and Alloys, The TPRC Data Series*, 1970, vol. 4, p. 511.
11. W.J. Parker, R.J. Jenkins, C.P. Butler, and G.L. Abbott: *J. Appl. Phys.*, 1961, vol. 32, p. 1679.
12. G. Bräuer, L. Dusza, and B. Schulz: *Interceramics*, 1992, vol. 41, p. 7.
13. L. Dusza: “Wärmetransport—Modelle zur Bestimmung der Temperaturleitfähigkeit von Werkstoffen mit der instationären Laser Flash Methode,” *Wissenschaftlicher Bericht (Scientific Report) FZKA 5820*, Forschungszentrum Karlsruhe GmbH, 1996.